High and low expression of the hyperpolarization activated current (I_h) in mouse CA1 stratum oriens interneurons.

Lauren T. Hewitt, Gregory J. Ordemann and Darrin H. Brager

Department of Neuroscience, Institute for Neuroscience
University of Texas at Austin
Austin, TX 78712

Corresponding author: dbrager@mail.clm.utexas.edu

Running Title: Excitability of CA1 interneurons

Keywords: hippocampus, spike frequency adaptation, K-means clustering, voltage-clamp

Key Points

- Spike frequency adaptation (SFA) was highly variable among stratum oriens interneurons
- Adapting stratum oriens interneurons were separated into two cell groups using multiple subthreshold and action potential parameters by cluster analysis
- Cells with strong SFA fired fewer action potentials for a given current injection, had lower input resistance and more sag and rebound compared to weak SFA cells
- The physiological differences were not correlated with neuron morphology, location in stratum oriens, or anatomical location along the dorsal-ventral axis of the hippocampus
- Voltage-clamp recordings revealed that strong SFA cells had higher density of the hyperpolarization activated current I_h compared to weak SFA cells

Abstract

Inhibitory interneurons are among the most diverse cell types in the brain; the hippocampus itself contains more than 28 different inhibitory interneurons. Interneurons are typically classified using a combination of physiological, morphological and biochemical observations. One broad separator is action potential firing: low threshold, regular spiking vs. higher threshold, fast spiking. We found that spike frequency adaptation (SFA) was highly heterogeneous in low threshold interneurons in the mouse stratum oriens region of area CA1. Analysis with a k-means clustering algorithm parsed the data set into two distinct clusters based on a constellation of physiological parameters and reliably sorted strong and weak SFA cells into different groups. Interneurons with strong SFA fired fewer action potentials across a range of current inputs and had lower input resistance compared to cells with weak SFA. Strong SFA cells also had higher sag and rebound in response to hyperpolarizing current injections. Morphological analysis shows no difference between the two cell types and the cell types did not segregate along the dorsal-ventral axis of the hippocampus. Strong and weak SFA cells were labeled in hippocampal slices from SST:cre Ai14 mice suggesting both cells express somatostatin. Voltage-clamp recordings showed hyperpolarization activated current I_h was significantly larger in strong SFA cells compared to weak SFA cells. We suggest that the strong SFA cell represents a previously

uncharacterized type of CA1 stratum oriens interneuron. Due to the combination of physiological parameters of these cells, we will refer to them as Low Threshold High I_h (LTH) cells.

Introduction

The elusive classification of the vast number of GABAergic interneuron subtypes has captivated neuroscientists for decades. The laminar organization of the hippocampus makes it an attractive model for studying circuit mechanisms, particularly because hippocampal interneurons have relatively reliable layer specific inputs and outputs (Cobb et al. 1995; Klausberger and Somogyi 2008; Royer et al. 2012). Hippocampal studies have revealed the extensive diversity of inhibitory interneurons poised to control network timing. Despite comprising merely 10-15% of hippocampal neurons, the remarkably precise activity of GABAergic inhibitory interneurons controls the timing and specificity of excitatory pyramidal cell output and orchestrates layered levels of synchrony in the hippocampal circuit (reviewed in (Bezaire and Soltesz 2013; Freundl and Buzsi 1996; Hájos et al. 2004; Pelkey et al. 2017)). To this end, interneurons play a critical role in facilitating hippocampal activity that ultimately underly complex hippocampal function such as contextual based learning, the formation of episodic memory, and spatial navigation (Lapray et al. 2012; Lovett-Barron et al. 2014; Murray et al. 2011).

Confident classification of the subtype of GABAergic interneurons is necessary in order to understand the particular role an interneuron plays in the local circuitry. Dissection of the functional roles of different inhibitory neurons has been historically difficult. Many studies utilize a three-part approach that entail describing the morphological, biochemical, and physiological properties (Ascoli et al. 2008; DeFelipe et al. 2013). Within the hippocampus, the CA1 region alone contains at least 28 previously described types of inhibitory interneurons located throughout all layers: stratum oriens, stratum pyramidale, stratum radiatum and stratum lacunosum-moleculare (Klausberger and Somogyi 2008). The stratum oriens (SO) of CA1 is home to a variety of regular spiking interneurons, including trilaminar cells, back propagating cells, and oriens-lacunosum moleculare (OLM) cells. OLM cells have a stereotyped morphology with dendrites extending perpendicular to

pyramidal cell dendrites along the CA3-subicular axis and an axon that projects through the stratum pyramidale and radiatum until it profusely branches within stratum lacunosum moleculare (Lacaille et al. 1987; Lacaille and Williams 1990; Maccaferri 2005; Maccaferri and McBain 1996). Through this anatomical arrangement, OLM cells coordinate a canonical feedback inhibitory circuit where CA1 neurons activate OLM cells which in turn inhibit the distal dendrites of CA1 pyramidal cells to gate incoming information from the entorhinal cortex via the temporoammonic pathway (Blasco-Ibáñez and Freund 1995; Klausberger 2009; Leão et al. 2012; Maccaferri and McBain 1995; Muller and Remy 2014). OLM cells exhibit tonic or mildly adapting firings characteristics and display sag and rebound responses during the onset and offset of hyperpolarization due to the expression of h-channels (Lupica et al. 2001; Maccaferri and McBain 1996). While OLM cells are well characterized, there are many interneurons throughout the brain discovered in patch-seq (Cadwell et al. 2016; Gouwens et al. 2020), single-cell recording (Tricoire et al. 2011), and single cell transcriptomic (Harris et al. 2018) experiments that remain uncharacterized. Descriptions of the subthreshold and active properties, and the ionic condutances that underly them, in these uncharacterized neurons are paramount to understanding how they contribute to the local circuitry.

In the present study we performed whole-cell recordings from interneurons in the stratum oriens that exhibited oblong cell bodies with dendrites extending along the CA3-subicular axis. We observed heterogenous spike frequency adaptation to depolarizing current injections. Cells with strong spike frequency adaptation (SFA) also had a lower input resistance, larger voltage sag and steeper rebound in response to hyperpolarizing current injections relative to cells with weak SFA. In contrast, single action potential properties were not correlated with SFA. We measured multiple action potential parameters in tandem with subthreshold properties and used a k-means clustering analysis which parsed the cells into two discrete clusters. Using voltage-clamp recordings, we found cells with strong SFA had larger hyperpolarization activated currents (I_h) compared to cells with weak SFA. We thus suggest the strongly adapting cells are distinct from weak SFA OLM cells. These strong SFA cells exhibit a low-threshold spiking phenotype and will fire action

78 potentials when given small amounts of current relative to other SO interneurons. We will
79 refer to these interneurons as Low-Threshold spiking High I_h cells (LTH).
80 Our data suggests that OLM and LTH cells exhibit distinct firing and subthreshold
81 properties, which are likely dictated from differences in ion channel and biochemical
82 expression profiles. It is a culmination of ion channel expression, inputs and outputs, and
83 intrinsic physiology that will ultimately dictate how a cell responds to different activity
84 states. It is clear that an appreciation for the highly diverse population of inhibitory
85 interneurons is critical to understanding hippocampal function.
86

87 **Methods**

88 *Slice Preparation:* All animal procedures were approved by the University of Texas at
89 Austin Institutional Animal Care and Use Committee. All mice were housed in a reverse
90 light dark cycle of 12hr on 12hr off with free access to food and water. Experiments used
91 male wild-type (JAX: C57/Bl6, stock #: 000664) and SST:cre Ai14 mice (JAX: SST:cre
92 (stock #:018973) crossed with Ai14 (stock #: 007914)) 2-4 months old (postnatal day 60 –
93 postnatal day 120). Mice were anesthetized with ketamine/xylazine (100/10 mg/kg) and
94 perfused through the heart with ice-cold saline consisting of (in mM): 2.5 KCl, 1.25
95 NaH_2PO_4, 25 $NaHCO_3$, 0.5 $CaCl_2$, 7 $MgCl_2$, 7 dextrose, 205 sucrose, 1.3 ascorbate and 3
96 sodium pyruvate (bubbled with 95% O_2/5% CO_2 to maintain pH at ~7.4). A vibrating tissue
97 slicer (Vibratome 3000, Vibratome Inc.) was used to make 300 µm thick parasagittal
98 sections from middle hippocampus. Slices were held in a chamber filled with artificial
99 cerebral spinal fluid (aCSF) consisting of (in mM): 125 NaCl, 2.5 KCl, 1.25 NaH_2PO_4, 25
100 $NaHCO_3$, 2 $CaCl_2$, 2 $MgCl_2$, 10 dextrose and 3 sodium pyruvate (bubbled with 95% O_2/5%
101 CO_2) for 30 minutes at 35°C and then at room temperature until the time of recording.

102 *Electrophysiology:* Slices were placed in a submerged, heated (33–34°C) recording
103 chamber and continually perfused (1−2 mL/minute) with aCSF 125 NaCl, 2.5 KCl, 1.25
104 NaH_2PO_4, 25 $NaHCO_3$, 2 $CaCl_2$, 2 $MgCl_2$, 10 dextrose and 3 sodium pyruvate (bubbled
105 with 95% O_2/5% CO_2). Synaptic transmission was blocked with 20 µM DNQX, 25 µM D-
106 AP5, and 2 µM Gabazine. Slices were visualized with a Zeiss AxioScope or Axioexaminer

107 under 60X magnification. All cells were located in the stratum oriens of CA1 and had
108 oblong cell bodies that ran along the subicular-CA3 axis. Experimenters selected cells with
109 oblong cell bodies, smaller than pyramidal cells, with dendrites extending in the CA3-
110 subcircular axis of the SO, perpendicular to pyramidal cell dendrites. Current injections of
111 100 pA and -80 pA were delivered to determine if the cells physiological properties were
112 consistent with 'regular spiking' adapting cells as described in (Maccaferri and McBain
113 1996)

114 *Current Clamp Recordings:* Internal recording solution contained (in mM): 135 K-
115 gluconate, 10 HEPES, 7 NaCl, 7 K2 phosphocreatine, 0.3 Na−GTP, 4 Mg−ATP (pH 7.3
116 with KOH). Current clamp data were acquired using a Dagan BVC−700 amplifier with
117 custom acquisition software written using Igor Pro (Wavemetrics) and sampled at 50 kHz,
118 filtered at 3 kHz and digitized by an ITC-18 (InstruTech) interface. Patch pipettes (4-6 MΩ)
119 were pulled from borosilicate glass. Pipette capacitance was compensated, and the bridge
120 balanced before each recording. Series resistance was monitored throughout each
121 experiment and maintained at approximately 15−35 MΩ. Cells with a series resistance >35
122 MΩ were omitted from the data set.

123 *Voltage Clamp Recordings:* The internal recording solution was the same as for current
124 clamp recordings (see above). Cells were first recorded in control aCSF (see above) in
125 current clamp mode to record trains of action potentials. Following current clamp
126 recording, voltage gated sodium, potassium and calcium currents were blocked with, 1 μM
127 TTX, 10 mM TEA, 5 mM 4AP, 200 μM $BaCl_2$, 100 μM $CdCl_2$. Cells were held at -30 mV
128 and inward currents were recorded in response to a series of 1-sec long hyperpolarzing
129 voltage commands (-50 to -130 mV in -10 mV steps). Voltage clamp data was acquired
130 using a Axopatch 200B amplifier (Molecular Devices) with Axograph or custom
131 acquisition software written using Igor Pro (Wavemetrics), digitized at 20 kHz and filtered
132 at 3 kHz. Patch pipettes (4-6 MΩ) were pulled from borosilicate glass.

133 *Drugs:* All drugs (Abcam pharmaceutical or Tocris) were prepared from 1000X stock
134 solutions in water.

135 *Post-hoc Neuron Visualization:* During whole-cell current clamp recordings, neurons were
136 filled with 0.4% neurobiotin. Upon completion of whole-cell recordings, slices were fixed
137 in 3% paraformaldehyde at 4 C overnight. Slices were then washed with 0.1 M PBS 3x for
138 20 min and place in a blocking buffer of 10% normal goat serum (NGS) and 0.5% triton in
139 PBS overnight at 4 C. Slices were then incubated in PBS containing 1% BSA and 1% NGS
140 with streptavidin conjugated to Alexa-488 (Invitrogen) for 24-48 hr at 4 C. Slices were then
141 rinsed in PBS 3x for 20 min and mounted in Flourmount. Slices were visualized on a
142 resonant scanning 2-photon system (Leica) and Z-stack images were taken. Cells were
143 reconstructed using the max projection of the Z-stack image and analyzed using the SNT
144 plug-in in ImageJ (NIH, https://imagej.net/SNT). (Arshadi et al. 2020)

145 *K-means clustering:* Neuron properties recorded in current clamp (resting membrane
146 potential, steady state R_N, max R_N, sag, rebound, ISI ratio, max firing frequency) were used
147 to determine if LTH and OLM cells would separate into distinct populations via k-means
148 clustering. Data was normalized via log transformation and subsequently used for analysis.
149 Using the NbClust package in R (Charrad et al. 2014) we determined the optimal number of
150 clusters for our data set. We then ran a principal components analysis (PCA) and
151 hierarchical clustering on our data and ultimately determined Euclidean distance using k-
152 means analysis.

153 *Data Analysis and statistical tests:* Electrophysiology data were analyzed using custom
154 analysis software written in IgorPro or AxoGraph. The input resistance (R_N) was calculated
155 from the linear portion of the current-voltage relationship in response to a family of 1500
156 ms current injections (-40 pA to +40 pA Δ10 pA). The FI curve was calculated from the
157 number of spikes elicited during a family of 1500 ms depolarizing current injections (25 pA
158 to 250 pA Δ25 pA). All statistical analyses (Student's t-test, ANOVA, repeated measures
159 ANOVA, and Pearson's correlation) were performed using Prism (Graphpad).
160

161 **Results**

162 ***Heterogeneity of spike frequency adaptation in low-threshold regular spiking stratum***
163 ***oriens interneurons***

164 We made whole-cell current clamp recordings from cells in stratum oriens of the
165 CA1 region of the hippocampus with oblong cell bodies and horizontally extending
166 dendrites. Low threshold interneurons were identified by having a resting potential close to
167 action potential threshold, an action potential half-width < 1.5ms, and an initial firing
168 frequency < 50 Hz. Stratum oriens interneurons typically display weak to no spike
169 frequency adaptation (Lacaille and Williams 1990; Maccaferri and McBain 1996; Williams
170 and Stuart 2003). Cells were held at -70 mV and depolarizing current injections were used
171 to elicit a train of action potentials. We first measured spike frequency adaptation (SFA) as
172 the ratio of the last interspike interval (ISI) relative to the first ISI (called the ISI ratio)
173 using the first current step that elicited multiple action potentials (Figure 1 A). We found
174 that SFA was highly heterogenous across cells with some showing weak SFA (ISI close to
175 1) and others showing strong SFA; the ISI ratio was not correlated with the resting
176 membrane potential. (SFA range across all cells: 1.1 – 6.5; Pearson's $r = -0.0015$, $p = 0.88$;
177 Figure 1 B). While ISI ratio is a reliable indicator of SFA, we sought a second method that
178 would reflect SFA across a range of current injections. Using a previously published
179 method for SFA in cortical neurons (Barkai and Hasselmo 1994), we fit a line to a plot of
180 the number of action potentials (spikes) as a function of normalized current injected (Figure
181 1 C). The area under the linear fit is the S-I value, an indication of adaptation. In agreement
182 with our measurement of ISI ratio, S-I value was highly heterogeneous across all cells
183 recorded (Figure 1 D).
184
185 ***Relationship of physiological parameters to spike frequency adaptation***
186 The subthreshold properties of hippocampal interneurons, including input resistance
187 (R_N) and voltage sag (max R_N / steady state R_N), can vary widely across the many
188 interneuron types (for review see (Pelkey et al. 2017)). We measured neuronal input
189 resistance (both maximum and steady state), voltage sag, and rebound and plotted each as a
190 function of SFA (ISI ratio). All four subthreshold parameters were correlated with cell
191 SFA. Maximum R_N (Pearson's $r = -0.6047$, $p = 0.0078$) and steady-state R_N (Pearson's $r = -$
192 0.6621, $p = 0.0028$) were negatively correlated with ISI ratio (Figure 2 A-C). Voltage sag
193 (Pearson's $r = 0.7822$, $p = 0.0002$) and rebound slope (Pearson's $r = -0.8941$, $p < 0.0001$)

194 were positively correlated with ISI ratio (Figure 2 D-F; note the negative r value for
195 rebound is because greater rebound is a more negative slope). Like subthreshold properties,
196 action potential properties can vary widely across hippocampal interneurons (for review see
197 (Pelkey et al. 2017)). Unlike subthreshold properties however, there was no correlation
198 between action potential threshold (Pearson's r = 0.2555; p = 0.3223), action potential half-
199 width (Pearson's r = 0.1201; p = 0.6462), action potential maximum dV/dt (Pearson's r = -
200 0.0637; p = 0.8081), or minimum dV/dt (Pearson's r = 0.1396; p = 0.5931) (Figure 2 G-L).
201
202 ***Clustering of heterogenous SFA interneurons***
203 We used these physiological parameters and a k-means clustering algorithm to
204 investigate whether the stratum oriens interneurons we recorded could be separated into
205 functionally distinct categories (Table 1; Figure 3 A). First, we determined the optimal
206 number of clusters given our data set. Our analyses in NbClust in R (Charrad et al. 2014)
207 revealed 2 clusters were optimal (k=2, Figure 3 B). Our data set neatly partitioned into two
208 distinct clusters based off of these physiological characteristics (Figure 3 C-E). Given the
209 large sag and rebound, consistent with the hyperpolarization activated current I_h, and strong
210 SFA associated with cluster 2, we will tentatively refer to these cells as Low Threshold
211 High I_h (LTH) interneurons and refer to cells in cluster 1 as canonical OLM interneurons.
212 We observed OLM (weak SFA) and LTH (strong SFA) neurons with roughly equal
213 probabilities, indicating LTH cells may not be simply a small population of SO
214 interneurons (OLM 10/18 cells, LTH 8/18 cells). Based on the two clusters produced by k-
215 means clustering, we compared the action potential and subthreshold properties between
216 these two groups.

K Means Chart	RMP (mV)	Rebound	ISI Ratio	Sag	R_N SS	R_N Max	Max Firing
LTH	-54 ± 1.35	-0.32 ± 0.04	4.16 ± 0.02	1.22 ± 0.03	295 ± 23.47	360 ± 28.06	43 ± 3.52
OLM	-52 ± 0.97	-0.04 ± 0.01	1.58 ± 0.03	1.03 ± 0.01	469 ± 31.21	487 ± 32.13	63 ± 4.51

217 **Table 1:** Table of the parameters used in the k-means clustering algorithm from Figure 3.
218 The analysis used the resting membrane potential (RMP, mV), rebound (mV/mV), ISI ratio
219 (first ISI/last ISI), sag (R_N SS / R_N Max), steady state input resistance (R_N SS, Mega Ohm),
220 maximum input resistance (R_N Max, Mega Ohm), and max firing rate (Hz).
221
222 ***Active properties***
223 The results of our clustering analysis suggest our recordings from stratum oriens
224 interneurons can be divided into at least two groups based on physiological characteristics.
225 We next asked if the two groups produced by k-means clustering had different intrinsic
226 properties. We measured action potential firing across a range of depolarizing current
227 injection amplitudes. We found that OLM cells fire significantly more action potentials
228 compared to LTH cells (Figure 4 A-B; repeated measures ANOVA, main effect of cell type
229 ($F(9, 144) = 279.3$; $p = 0.0023$)). We isolated the first action potential elicited by the
230 smallest current injection for analysis (Figure 4 C-D). Consistent with our observations in
231 Figure 2, there was no significant difference in action potential threshold, half-width, min
232 or max dV/dt between OLM and LTH cells (Figure 4 E-H). These data suggest the sodium
233 and potassium conductances that contribute to the first action potential were not
234 significantly different between OLM and LTH cells.
235
236 ***Passive Properties***
237 There was no difference in resting membrane potential between OLM and LTH
238 cells (Figure 1 B). In agreement with previous reports on stratum oriens interneurons, both
239 OLM and LTH cells had resting membrane potentials more depolarized compared to
240 hippocampal pyramidal cells (Maccaferri and McBain 1996; Tricoire et al. 2011). OLM
241 cells have significantly higher input resistance (R_N) compared to LTH cells (Figure 5 B).
242 OLM neurons express h-channels, which is made evident by small voltage sag during the
243 onset and rebound during the offset of hyperpolarizing current injections (Lupica et al.
244 2001; Maccaferri and McBain 1996; Zemankovics et al. 2010). We measured sag as the
245 difference between the maximum voltage and steady state as indicated by the arrows.
246 (Figure 5 C; grey indicates LTH cells and black indicates OLM cells). While both OLM

247 and LTH cells display sag and rebound, both the sag and rebound were significantly larger
248 in LTH cells compared to OLM cells (Figure 5 D-F).
249
250 ***OLM and LTH cells express SST***
251 The use of transgenic mouse lines to target interneuron subtypes has been critical to
252 furthering the study of physiological properties of different interneurons (Taniguchi et al.
253 2011). We recorded fluorescent cells from somatostatin:cre Ai14 mice (SST:cre Ai14) to
254 determine if OLM and LTH cells could both be found in the fluorescent cell population,
255 indicating the expression of somatostatin. We recorded from 13 fluorescent cells
256 (representative images Figure 6 B and D), post hoc analysis of subthreshold and SFA
257 properties indicated 7/13 cells were LTH cells and 6/13 cells were OLM cells. All LTH
258 cells exhibited strong SFA, sag, and rebound properties (Figure 6 A) and had oblong cell
259 bodies in the stratum oriens (Figure 6 B). OLM cells exhibited weak SFA spiking profile
260 with moderate sag (Figure 6 C). Our results suggest the use of SST:cre Ai14 mouse lines
261 indeed lead to sampling a heterogenous population of interneuron subtypes (also indicated
262 in (Hu et al. 2013)), particularly in the stratum oriens where both OLM and LTH cells were
263 found in this mouse model.
264
265 ***OLM and LTH cells have similar neuronal morphology***
266 The properties of hippocampal pyramidal neurons vary along the dorsal ventral axis
267 of the hippocampus (Dougherty et al. 2012; Kim and Johnston 2015; Malik et al. 2016;
268 Ordemann et al. 2019). More recently, OLM cells were shown to have distinct intrinsic
269 physiological properties depending on the dorsal ventral location of the cell (Hilscher et al.
270 2019). To determine if the dorsal ventral location of our recordings biased our findings, we
271 mapped our slices to examine their dorsal ventral position within the hippocampus (Malik
272 et al. 2016). Our analysis confirms that our recordings were made from slices taken from
273 the middle hippocampus and that there was no significant difference in the dorsal ventral
274 location of our OLM and LTH cell recordings (Figure 7 A and C). We analyzed the
275 position of our recovered and reconstructed neurons and observed no difference in where
276 OLM and LTH cells are found in the subbicular-CA3 axis of the hippocampus (Figure 7 B).

277 Differences in neuronal morphology will strongly influence physiology. Recorded cells
278 were filled with neurobiotin and reconstructed (Figure 7 D). We did not observe gross
279 differences in the somato-dendritic morphological structure of OLM and LTH cells (Figure
280 7 E). Both cells had oblong cell bodies in the stratum oriens with dendrites extending along
281 the CA3- subicular axis. A few LTH cells did seem to have dendrites that extended into the
282 pyramidal layer (2 of 6 reconstructions). Axons recovered from OLM cells showed typical
283 extensive branching in the SLM (2 of 5 reconstructions) while axons recovered from LTH
284 cells seemed to also descend out of the pyramidal layer. (2 of 6 reconstructions).
285
286 ***Higher I_h density in LTH cells***
287 Our current-clamp recordings showed that OLM cells have higher R_N and smaller
288 sag and rebound compared to LTH cells. OLM cells were previously shown to have
289 hyperpolarization activated non-selective cation channels (I_h; (Lupica et al. 2001;
290 Maccaferri and McBain 1996; Matt et al. 2011)). Based on the larger sag and rebound, we
291 hypothesized that LTH cells had higher I_h compared to OLM cells. We used a combined
292 current-clamp/voltage-clamp approach to measure the density of I_h in OLM and LTH cells
293 (Figure 8 A). After we used depolarizing current injections to evoke action potential firing
294 to measure ISI ratio, we switched to voltage clamp and bath applied 1 μM TTX to block
295 voltage-gated Na^+ channels; 10 mM TEA, 5 mM 4-AP and 200 μM $BaCl_2$ to block voltage-
296 gated K^+ channels; and 100 μM $CdCl_2$ to block voltage-gated calcium channels. In order to
297 compare to previously published results, we used the same whole-cell voltage clamp
298 approach described in Maccafferi and McBain 1996. We used a series of hyperpolarizing
299 voltage steps to elicit a slowly activating inward current (Figure 8 B-C). The density of I_h
300 was significantly higher in LTH cells compared to OLM cells (Figure 8, D-E, black
301 circles). The current was completely blocked by the h-channel blocker ZD7288 (50 μM)
302 (Figure 8 D-E, grey circles). These results suggest that the subthreshold differences
303 between OLM and LTH cells were due in part to the differential expression of the
304 hyperpolarization activated current I_h.
305
306

307 **Discussion**

308 Interneurons exhibit a wide range of physiological and molecular profiles leading
309 many researchers to question what defines a specific interneuron subtype. Here we use a
310 combination of physiological, morphological, and biochemical approaches to identify a
311 previously uncharacterized subtype of hippocampal stratum oriens interneuron, LTH cells.
312 We identified a number of different intrinsic physiological properties between OLM and
313 LTH cells. LTH cells fire fewer action potentials in response to depolarizing current steps
314 when compared to OLM cells. Single action potential analysis revealed no differences in
315 threshold, amplitude, half-width, or min/max dV/dt, which suggests that the ion channel
316 conductances underlying these properties may not be significantly different between LTH
317 and OLM cells. We found that the input resistance of LTH was significantly lower
318 compared to OLM cells. While the decrease in firing may be related to the lower input
319 resistance of LTH cells, our analysis does not capture how the spike waveform changes
320 with concurrent spikes across the current step, which may reveal an underlying
321 conductance that increases the adaptation of LTH cells leading to a decrease in spikes.
322 Voltage sag was steeper and rebound larger in LTH cells compared to OLM cells. Sag and
323 rebound are current clamp indicators of h-channel function leading us to hypothesize that
324 LTH cells have higher h-channel current compared to OLM neurons. Indeed, we found that
325 I_h density is significantly higher in LTH cells compared to OLM cells.
326

327 ***Ion channel contributions to LTH neuron intrinsic properties***

328 These intrinsic properties of neurons shape the integration of synaptic inputs,
329 precision of action potential output, and contribution to the local circuitry. Our data show
330 LTH cells have significantly higher density of I_h resulting in altered subthreshold properties
331 (R_N, sag, and rebound). Differences in I_h between OLM and LTH cells suggest key
332 differences in the ability of LTH neurons to integrate synaptic activity and trigger action
333 potential output. The lower input resistance of LTH cells suggest that larger synaptic
334 currents would be required to fire action potentials. In addition, the higher density of h-
335 channels would also limit the summation of synaptic inputs. Taken together, this suggests

336 that both magnitude and temporal frequency of synaptic inputs would need to be higher to
337 drive LTH cells to fire action potentials compared to OLM cells.
338 The higher density of I_h would be expected to lower input resistance and depolarize
339 the resting membrane potential (Lupica et al. 2001).While we did find that the input
340 resistance of LTH cells was lower compared to OLM cells, there was no difference in
341 resting membrane potential. This could indicate that there is not as much I_h at rest in LTH
342 cells or there are likely additional channels active at or near the resting membrane potential
343 may be different between LTH and OLM cells. LTH cells exhibit stronger SFA compared
344 to OLM cells. It is not likely differences in I_h density account for the SFA, due to h-
345 channels not being active during large depolarizations. Several different potassium
346 channels can contribute to SFA including Ca^{2+}-activated BK and SK channels, and m-
347 channels (Gu et al. 2005, 2007; Peters et al. 2005). Further study is required to determine if
348 there are differences in the expression and or function of these channels between LTH and
349 OLM cells.
350
351 ***LTH Interneuron Identity***
352 Given the vast diversity of hippocampal interneurons, it is not surprising to find
353 subtypes of interneurons that lack characterization. A previous study dissected different
354 interneuron types based on developmental lineage and uncovered many uncharacterized
355 interneurons (Tricoire et al. 2011). Recent momentous undertakings have revealed that
356 many cell types still lack proper descriptions (Gouwens et al. 2020; Harris et al. 2018).
357 LTH cells appear to be one of these interneuron subtypes that have not been thoroughly
358 characterized. Trilaminar and back propagating interneurons are also found in CA1 SO and
359 present with oblong cells bodies with dendrites that extend perpendicular to pyramidal CA1
360 neurons (Sik et al. 1994, 1995). It is unlikely that LTH cells are trilaminar cells considering
361 trilaminar cells do not express a sag and rebound response (Gloveli et al. 2005). Back
362 propagating interneurons are typically found in the alveus of CA1, but can also been seen in
363 CA1 SO. These particular interneurons have an axon that extends into CA3. The
364 morphological analysis of the LTH cells in our study did not seem to have any axon
365 processes in CA3, however, this could be due to an incomplete fill of the axon or the axon

366 not being planar in our slice preparation. A paper from Zemankovic et al. in 2010 grouped
367 together cells in the CA1 SO that seemed to be projecting neurons with similar
368 physiological properties and diverse morphological properties (OR group). This group of
369 cells exhibits a steeper sag and rebound response to depolarize steps when compared to
370 OLM cells. However, whole cell voltage clamp study of I_h in OR and OLM neurons did not
371 reveal any significant differences (Zemankovics et al. 2010). This could be due to the OR
372 group of neurons being heterogenous indicating LTH cells could potentially be a part of the
373 neurons recorded in the OR group. LTH neurons have very likely been recorded from and
374 included in many studies, here we present a detailed characterization of the intrinsic
375 properties of LTH cells to create a foundation for understanding how these neurons may
376 impact hippocampal circuitry.
377
378 ***Contrasting LTH and OLM interneurons***
379 It is likely the case, as in many biological systems, that interneuron subtypes cannot
380 be split into discrete subtypes, but instead exist on an axis of properties that define their
381 role in information processing. While many interneuron subtypes do exist on graded axes of
382 properties, given our current data, it seems unlikely for LTH cells to be a subset of the
383 OLM interneurons. While the OLM cells typically originate from the medial ganglionic
384 eminence, a subtype of OLM cells originate from the central ganglionic eminence
385 (Chittajallu et al. 2013; Winterer et al. 2019). These two subclasses of OLM cells are
386 indistinguishable based on physiology. In contrast, we found marked differences in both the
387 firing patterns and subthreshold physiological properties between LTH and OLM cells.
388 OLM interneuron properties can vary based on the dorsal/ventral location of the cell.
389 Ventral OLM cells exhibit more adapting firing rates compared to dorsal cells. Dorsal OLM
390 cells also show a steeper sag response compared to ventral interneurons (Hilscher et al.
391 2019). We show that both LTH and OLM cells are found in the same dorsal/ventral extent
392 within the middle region of the hippocampus. We further demonstrate a separation of LTH
393 cells from OLM cells based on sampled physiological properties with a k-means clustering
394 algorithm. Taken together, we suggest that LTH cells are a separate class of stratum oriens
395 interneuron.

396

397 ***Somatostatin expression and morphology of LTH interneurons***

398 While biochemical markers such as parvalbumin (PV) and somatostatin (SST) are
399 traditionally used to differentiate subtypes of hippocampal interneurons, many cells express
400 both PV and SST or other combinations of common inhibitory interneuron markers
401 (Losonczy et al. 2002; Maccaferri et al. 2000; Tricoire et al. 2011). We observed both LTH
402 and OLM interneurons in SST:cre Ai14 leading us to believe LTH cells express SST.
403 Action potential firing is also used to separate classes of interneurons as 'fast spiking' vs
404 'regular spiking'. Some interneuron classes have distinctive dendritic and axonal arbors but
405 the number of interneurons that can identified by morphology alone, particularly in under
406 characterized interneurons, is limited (Ascoli et al. 2008; DeFelipe et al. 2013; Maccaferri
407 and Lacaille 2003). LTH cells may have an axon that is not planar in our current slice
408 preparation, indeed it would be interesting to investigate the full extent of LTH neuron
409 morphology, particularly the axon, using modern tracing methods. It has become
410 increasingly common to determine the genetic profile of inhibitory interneurons as well, we
411 have gained many insights from recent literature exploring an array of genetic markers of
412 interneuron subtypes that have recorded physiological and reconstructed morphological
413 properties (as in (Gouwens et al. 2020)). Large strides in genetic and big data techniques
414 have allowed scientists to study inhibitory interneurons in exquisite detail. Genetic mouse
415 models and intersectional genetics have made targeted approaches accessible to begin
416 untangling interneuron subtypes functional role in circuits. While we do not show the full
417 molecular profile of LTH cells here, it will be interesting to determine if additional key
418 interneuron markers, if any, are expressed. It is the constellation of properties exhibited by
419 a neuron that determines its function in a circuit. Taking all of these properties into account
420 may be necessary to describe how OLM and LTH cells are both different and related to
421 each other.

Acknowledgements:
We thank Dr. Chris McBain for generously providing protocols for slice processing for reconstructions, assistance with the k-means clustering code, and helpful discussion on this manuscript, Jarod Talbot for conducting the dorsal ventral analysis on processed slices, Dr. Richard Gray for assistance with analysis programs, Meagan Volquardsen for genotyping and mouse colony management, members of the Johnston lab for helpful comments and lively discussion on this manuscript, and to Emily Aster Jones and Jessica Chancey for helpful review of our manuscript. This work was supported by the National Institutes of Health grant RO1 MH100510 (DHB) and the National Science Foundation Graduate Research Fellowship Program (LTH).

Author Contributions:
L.T.H. and D.H.B. designed experiments; L.T.H., G.J.O, and D.H.B. acquired data; L.T.H., G.J.O, and D.H.B. analyzed data; L.T.H. and D.H.B. interpreted results of experiments; L.T.H. and D.H.B. prepared figures; L.T.H. and D.H.B. drafted manuscript; L.T.H., G.J.O., and D.H.B. edited and revised manuscript.

References

1. **Arshadi C**, **Günther U**, **Eddison M**, **Harrington KIS**, **Ferreira TA**. SNT: A Unifying Toolbox for Quantification of Neuronal Anatomy. Neuroscience.

2. **Ascoli GA**, **Alonso-Nanclares L**, **Anderson SA**, **Barrionuevo G**, **Benavides-Piccione R**, **Burkhalter A**, **Buzsáki G**, **Cauli B**, **DeFelipe J**, **Fairén A**, **Feldmeyer D**, **Fishell G**, **Fregnac Y**, **Freund TF**, **Gardner D**, **Gardner EP**, **Goldberg JH**, **Helmstaedter M**, **Hestrin S**, **Karube F**, **Kisvárday ZF**, **Lambolez B**, **Lewis DA**, **Marin O**, **Markram H**, **Muñoz A**, **Packer A**, **Petersen CCH**, **Rockland KS**, **Rossier J**, **Rudy B**, **Somogyi P**, **Staiger JF**, **Tamas G**, **Thomson AM**, **Toledo-Rodriguez M**, **Wang Y**, **West DC**, **Yuste R**, **The Petilla Interneuron Nomenclature Group (PING)**. Petilla terminology: nomenclature of features of GABAergic interneurons of the cerebral cortex. *Nature Reviews Neuroscience* 9: 557–568, 2008.

3. **Barkai E**, **Hasselmo ME**. Modulation of the input/output function of rat piriform cortex pyramidal cells. *Journal of Neurophysiology* 72: 644–658, 1994.

4. **Bezaire MJ**, **Soltesz I**. Quantitative Assessment of CA1 Local Circuits: Knowledge Base for Interneuron-Pyramidal Cell Connectivity. *Hippocampus* 23: 751–785, 2013.

5. **Blasco-Ibáñez JM**, **Freund TF**. Synaptic Input of Horizontal Interneurons in Stratum Oriens of the Hippocampal CA1 Subfield: Structural Basis of Feed-back Activation. *European Journal of Neuroscience* 7: 2170–2180, 1995.

6. **Cadwell CR**, **Palasantza A**, **Jiang X**, **Berens P**, **Deng Q**, **Yilmaz M**, **Reimer J**, **Shen S**, **Bethge M**, **Tolias KF**, **Sandberg R**, **Tolias AS**. Electrophysiological, transcriptomic and morphologic profiling of single neurons using Patch-seq. *Nature Biotechnology* 34: 199–203, 2016.

7. **Charrad M**, **Ghazzali N**, **Boiteau V**, **Niknafs A**. NbClust: An R Package for Determining the Relevant Number of Clusters in a Data Set. *Journal of Statistical Software* 61: 1–36, 2014.

8. **Chittajallu R**, **Craig MT**, **McFarland A**, **Yuan X**, **Gerfen S**, **Tricoire L**, **Erkkila B**, **Barron SC**, **Lopez CM**, **Liang BJ**, **Jeffries BW**, **Pelkey KA**, **McBain CJ**. Dual origins of functionally distinct O-LM interneurons revealed by differential 5-HT_{3A}R expression. *Nature Neuroscience* 16: 1598–1607, 2013.

9. **Cobb SR**, **Buhl EH**, **Halasy K**, **Paulsen O**, **Somogyi P**. Synchronization of neuronal activity in hippocampus by individual GABAergic interneurons. *Nature* 378: 75–78, 1995.

10. **DeFelipe J**, **López-Cruz PL**, **Benavides-Piccione R**, **Bielza C**, **Larrañaga P**, **Anderson S**, **Burkhalter A**, **Cauli B**, **Fairén A**, **Feldmeyer D**, **Fishell G**,

Fitzpatrick D, **Freund TF**, **González-Burgos G**, **Hestrin S**, **Hill S**, **Hof PR**, **Huang J**, **Jones EG**, **Kawaguchi Y**, **Kisvárday Z**, **Kubota Y**, **Lewis DA**, **Marín O**, **Markram H**, **McBain CJ**, **Meyer HS**, **Monyer H**, **Nelson SB**, **Rockland K**, **Rossier J**, **Rubenstein JLR**, **Rudy B**, **Scanziani M**, **Shepherd GM**, **Sherwood CC**, **Staiger JF**, **Tamás G**, **Thomson A**, **Wang Y**, **Yuste R**, **Ascoli GA**. New insights into the classification and nomenclature of cortical GABAergic interneurons. *Nat Rev Neurosci* 14: 202–216, 2013.

11. **Dougherty KA**, **Islam T**, **Johnston D**. Intrinsic excitability of CA1 pyramidal neurones from the rat dorsal and ventral hippocampus. *J Physiol* 590: 5707–5722, 2012.

12. **Freundl TF**, **Buzsi G**. Interneurons of the hippocampus. *Hippocampus* 6: 347–470, 1996.

13. **Gloveli T**, **Dugladze T**, **Saha S**, **Monyer H**, **Heinemann U**, **Traub RD**, **Whittington MA**, **Buhl EH**. Differential involvement of oriens/pyramidale interneurones in hippocampal network oscillations in vitro. *The Journal of Physiology* 562: 131–147, 2005.

14. **Gouwens NW**, **Sorensen SA**, **Baftizadeh F**, **Budzillo A**, **Lee BR**, **Jarsky T**, **Alfiler L**, **Baker K**, **Barkan E**, **Berry K**, **Bertagnolli D**, **Bickley K**, **Bomben J**, **Braun T**, **Brouner K**, **Casper T**, **Crichton K**, **Daigle TL**, **Dalley R**, **de Frates RA**, **Dee N**, **Desta T**, **Lee SD**, **Dotson N**, **Egdorf T**, **Ellingwood L**, **Enstrom R**, **Esposito L**, **Farrell C**, **Feng D**, **Fong O**, **Gala R**, **Gamlin C**, **Gary A**, **Glandon A**, **Goldy J**, **Gorham M**, **Graybuck L**, **Gu H**, **Hadley K**, **Hawrylycz MJ**, **Henry AM**, **Hill D**, **Hupp M**, **Kebede S**, **Kim TK**, **Kim L**, **Kroll M**, **Lee C**, **Link KE**, **Mallory M**, **Mann R**, **Maxwell M**, **McGraw M**, **McMillen D**, **Mukora A**, **Ng L**, **Ng L**, **Ngo K**, **Nicovich PR**, **Oldre A**, **Park D**, **Peng H**, **Penn O**, **Pham T**, **Pom A**, **Popović Z**, **Potekhina L**, **Rajanbabu R**, **Ransford S**, **Reid D**, **Rimorin C**, **Robertson M**, **Ronellenfitch K**, **Ruiz A**, **Sandman D**, **Smith K**, **Sulc J**, **Sunkin SM**, **Szafer A**, **Tieu M**, **Torkelson A**, **Trinh J**, **Tung H**, **Wakeman W**, **Ward K**, **Williams G**, **Zhou Z**, **Ting JT**, **Arkhipov A**, **Sümbül U**, **Lein ES**, **Koch C**, **Yao Z**, **Tasic B**, **Berg J**, **Murphy GJ**, **Zeng H**. Integrated Morphoelectric and Transcriptomic Classification of Cortical GABAergic Cells. *Cell* 183: 935-953.e19, 2020.

15. **Gu N**, **Vervaeke K**, **Hu H**, **Storm JF**. Kv7/KCNQ/M and HCN/h, but not KCa2/SK channels, contribute to the somatic medium after-hyperpolarization and excitability control in CA1 hippocampal pyramidal cells. *J Physiol* 566: 689–715, 2005.

16. **Gu N**, **Vervaeke K**, **Storm JF**. BK potassium channels facilitate high-frequency firing and cause early spike frequency adaptation in rat CA1 hippocampal pyramidal cells. *The Journal of Physiology* 580: 859–882, 2007.

17. **Hájos N**, **Pálhalmi J**, **Mann EO**, **Németh B**, **Paulsen O**, **Freund TF**. Spike Timing of Distinct Types of GABAergic Interneuron during Hippocampal Gamma Oscillations In Vitro. *J Neurosci* 24: 9127–9137, 2004.

18. **Harris KD**, **Hochgerner H**, **Skene NG**, **Magno L**, **Katona L**, **Gonzales CB**, **Somogyi P**, **Kessaris N**, **Linnarsson S**, **Hjerling-Leffler J**. Classes and continua of hippocampal CA1 inhibitory neurons revealed by single-cell transcriptomics. *PLOS Biology* 16: e2006387, 2018.

19. **Hilscher MM**, **Nogueira I**, **Mikulovic S**, **Kullander K**, **Leão RN**, **Leão KE**. Chrna2-OLM interneurons display different membrane properties and h-current magnitude depending on dorsoventral location. *Hippocampus* hipo.23134, 2019.

20. **Hu H**, **Cavendish JZ**, **Agmon A**. Not all that glitters is gold: off-target recombination in the somatostatin–IRES-Cre mouse line labels a subset of fast-spiking interneurons. *Front Neural Circuits* 7, 2013.

21. **Kim CS**, **Johnston D**. A1 adenosine receptor-mediated GIRK channels contribute to the resting conductance of CA1 neurons in the dorsal hippocampus. *J Neurophysiol* 113: 2511–2523, 2015.

22. **Klausberger T**. GABAergic interneurons targeting dendrites of pyramidal cells in the CA1 area of the hippocampus. *European Journal of Neuroscience* 30: 947–957, 2009.

23. **Klausberger T**, **Somogyi P**. Neuronal Diversity and Temporal Dynamics: The Unity of Hippocampal Circuit Operations. *Science* 321: 53–57, 2008.

24. **Lacaille J**, **Mueller A**, **Kunkel D**, **Schwartzkroin P**. Local circuit interactions between oriens/alveus interneurons and CA1 pyramidal cells in hippocampal slices: electrophysiology and morphology. *J Neurosci* 7: 1979–1993, 1987.

25. **Lacaille JC**, **Williams S**. Membrane properties of interneurons in stratum oriens-alveus of the CA1 region of rat hippocampus in vitro. *Neuroscience* 36: 349–359, 1990.

26. **Lapray D**, **Lasztoczi B**, **Lagler M**, **Viney TJ**, **Katona L**, **Valenti O**, **Hartwich K**, **Borhegyi Z**, **Somogyi P**, **Klausberger T**. Behavior-dependent specialization of identified hippocampal interneurons. *Nat Neurosci* 15: 1265–1271, 2012.

27. **Leão RN**, **Mikulovic S**, **Leão KE**, **Munguba H**, **Gezelius H**, **Enjin A**, **Patra K**, **Eriksson A**, **Loew LM**, **Tort ABL**, **Kullander K**. OLM interneurons differentially modulate CA3 and entorhinal inputs to hippocampal CA1 neurons. *Nature Neuroscience* 15: 1524–1530, 2012.

28. **Losonczy A**, **Zhang L**, **Shigemoto R**, **Somogyi P**, **Nusser Z**. Cell type dependence and variability in the short-term plasticity of EPSCs in identified mouse hippocampal interneurones. *The Journal of Physiology* 542: 193–210, 2002.

29. **Lovett-Barron M**, **Kaifosh P**, **Kheirbek MA**, **Danielson N**, **Zaremba JD**, **Reardon TR**, **Turi GF**, **Hen R**, **Zemelman BV**, **Losonczy A**. Dendritic Inhibition in the Hippocampus Supports Fear Learning. *Science* 343: 857–863, 2014.

30. **Lupica CR**, **Bell JA**, **Hoffman AF**, **Watson PL**. Contribution of the Hyperpolarization-Activated Current (I_h) to Membrane Potential and GABA Release in Hippocampal Interneurons. *Journal of Neurophysiology* 86: 261–268, 2001.

31. **Maccaferri G**. Stratum oriens horizontal interneurone diversity and hippocampal network dynamics. *The Journal of Physiology* 562: 73–80, 2005.

32. **Maccaferri G**, **David J**, **Roberts B**, **Szucs P**, **Cottingham CA**, **Somogyi P**. Cell surface domain specific postsynaptic currents evoked by identified GABAergic neurones in rat hippocampus in vitro. *The Journal of Physiology* 524: 91–116, 2000.

33. **Maccaferri G**, **Lacaille J-C**. Interneuron Diversity series: Hippocampal interneuron classifications--making things as simple as possible, not simpler. *Trends Neurosci* 26: 564–571, 2003.

34. **Maccaferri G**, **McBain CJ**. Passive propagation of LTD to stratum oriens-alveus inhibitory neurons modulates the temporoammonic input to the hippocampal CA1 region. *Neuron* 15: 137–145, 1995.

35. **Maccaferri G**, **McBain CJ**. The hyperpolarization-activated current (Ih) and its contribution to pacemaker activity in rat CAI hippocampal stratum oriens-alveus interneurones. *J Physiol* 12, 1996.

36. **Malik R**, **Dougherty KA**, **Parikh K**, **Byrne C**, **Johnston D**. Mapping the electrophysiological and morphological properties of CA1 pyramidal neurons along the longitudinal hippocampal axis. *Hippocampus* 26: 341–361, 2016.

37. **Matt L**, **Michalakis S**, **Hofmann F**, **Hammelmann V**, **Ludwig A**, **Biel M**, **Kleppisch T**. HCN2 channels in local inhibitory interneurons constrain LTP in the hippocampal direct perforant path. *Cell Mol Life Sci* 68: 125–137, 2011.

38. **Muller C**, **Remy S**. Dendritic inhibition mediated by O-LM and bistratified interneurons in the hippocampus. *Front Synaptic Neurosci* 6, 2014.

39. **Murray AJ**, **Sauer J-F**, **Riedel G**, **McClure C**, **Ansel L**, **Cheyne L**, **Bartos M**, **Wisden W**, **Wulff P**. Parvalbumin-positive CA1 interneurons are required for spatial working but not for reference memory. *Nat Neurosci* 14: 297–299, 2011.

40. **Ordemann GJ**, **Apgar CJ**, **Brager DH**. D-type potassium channels normalize action potential firing between dorsal and ventral CA1 neurons of the mouse hippocampus. *Journal of Neurophysiology* 121: 983–995, 2019.

41. **Pelkey KA**, **Chittajallu R**, **Craig MT**, **Tricoire L**, **Wester JC**, **McBain CJ**. Hippocampal GABAergic Inhibitory Interneurons. *Physiological Reviews* 97: 1619–1747, 2017.

42. **Peters HC**, **Hu H**, **Pongs O**, **Storm JF**, **Isbrandt D**. Conditional transgenic suppression of M channels in mouse brain reveals functions in neuronal excitability, resonance and behavior. *Nature Neuroscience* 8: 51–60, 2005.

43. **Royer S**, **Zemelman BV**, **Losonczy A**, **Kim J**, **Chance F**, **Magee JC**, **Buzsáki G**. Control of timing, rate and bursts of hippocampal place cells by dendritic and somatic inhibition. *Nat Neurosci* 15: 769–775, 2012.

44. **Sik A**, **Penttonen M**, **Ylinen A**, **Buzsaki G**. Hippocampal CA1 interneurons: an in vivo intracellular labeling study. *J Neurosci* 15: 6651–6665, 1995.

45. **Sik A**, **Ylinen A**, **Penttonen M**, **Buzsaki G**. Inhibitory CA1-CA3-hilar region feedback in the hippocampus. *Science* 265: 1722–1724, 1994.

46. **Taniguchi H**, **He M**, **Wu P**, **Kim S**, **Paik R**, **Sugino K**, **Kvitsani D**, **Fu Y**, **Lu J**, **Lin Y**, **Miyoshi G**, **Shima Y**, **Fishell G**, **Nelson SB**, **Huang ZJ**. A Resource of Cre Driver Lines for Genetic Targeting of GABAergic Neurons in Cerebral Cortex. *Neuron* 71: 995–1013, 2011.

47. **Tricoire L**, **Pelkey KA**, **Erkkila BE**, **Jeffries BW**, **Yuan X**, **McBain CJ**. A Blueprint for the Spatiotemporal Origins of Mouse Hippocampal Interneuron Diversity. *J Neurosci* 31: 10948–10970, 2011.

48. **Williams SR**, **Stuart GJ**. Voltage- and Site-Dependent Control of the Somatic Impact of Dendritic IPSPs. *J Neurosci* 23: 7358–7367, 2003.

49. **Winterer J**, **Lukacsovich D**, **Que L**, **Sartori AM**, **Luo W**, **Földy C**. Single-cell RNA-Seq characterization of anatomically identified OLM interneurons in different transgenic mouse lines. *European Journal of Neuroscience* n/a, 2019.

50. **Zemankovics R**, **Káli S**, **Paulsen O**, **Freund TF**, **Hájos N**. Differences in subthreshold resonance of hippocampal pyramidal cells and interneurons: the role of h-current and passive membrane characteristics. *The Journal of Physiology* 588: 2109–2132, 2010.

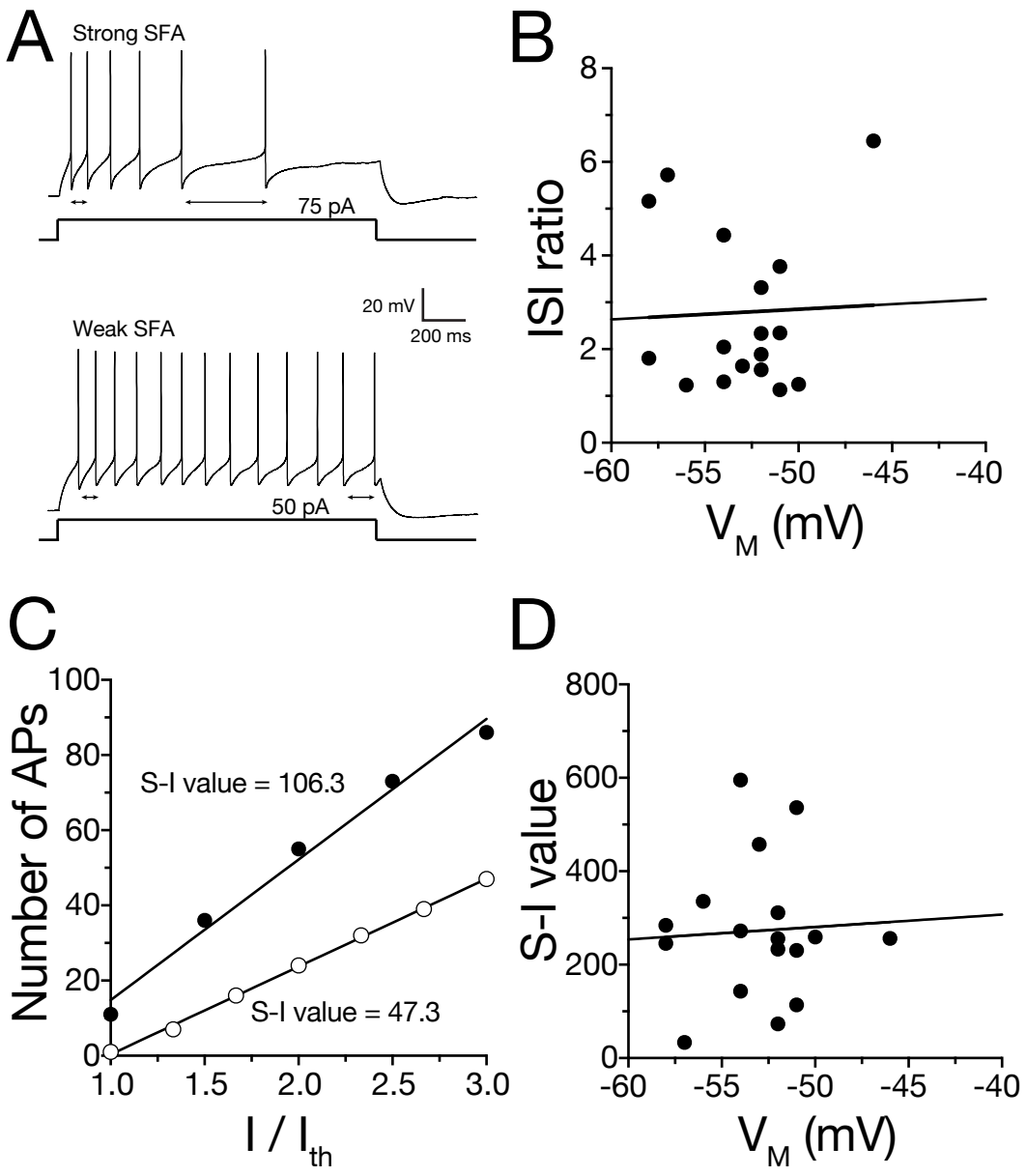

Figure 1: Spike frequency adaptation varies among stratum oriens interneurons A. Voltage traces from weak SFA and strong SFA cells showing the smallest current step to elicit action potentials. Note the strong spike frequency adaptation in the strong SFA cell. Cells were held at -70 mV. B. The ISI ratio does not have a significant relationship to the resting membrane potential (SFA range across all cells: 1.1 – 6.5; Pearson's r = -0.0015, p = 0.88). ISI ratio was determined by dividing the ISI between the last to spikes (arrow 1) by the ISI of the first two spikes (arrow two). C. Number of action potentials as a function of normalized current injected. The area under the curve (S-I value) indicates the strength of adaptation. D. S-I value is not correlated with VM (mV).

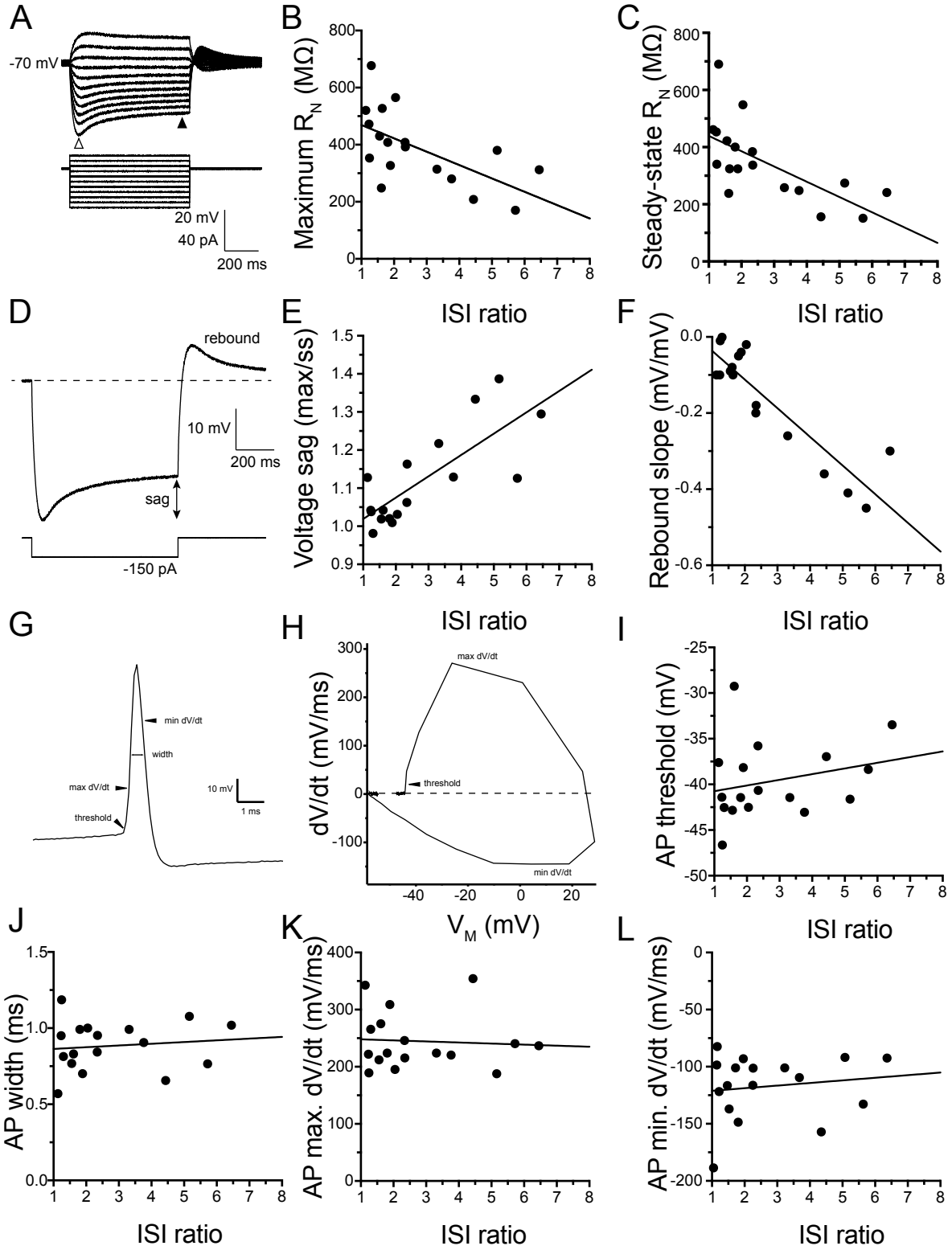

Figure 2: Relationship of physiological parameters to ISI ratio A. Example voltage traces indicating the measurements of maximum (open arrow) and steady state voltages (closed arrow) were taken. B-C. There is a strong correlation of steady state and maximum input resistance with the ISI ratio (Maximum RN (Pearson's r = -0.6047, p = 0.0078) and steady-state RN (Pearson's r = -0.6621, p = 0.0028)). D. example voltage traces of the voltage sag and rebound response. E-F. There is a strong relationship between the ISI ratio with voltage sag and rebound (Voltage sag (Pearson's r = 0.7822, p = 0.0002) and rebound slope (Pearson's r = -0.8941, p < 0.0001)). G. Example voltage trace of a single AP with arrows indicating where different properties are measured. H. Example phase plane plot of a single AP. Note where maximum dV/dt, minimum dV/dt, and AP threshold are indicated. I-L. Active properties measured from the first action potential. There is no relationship between AP threshold (Pearson's r = 0.2555; p = 0.3223), half-width (Pearson's r = 0.1201; p = 0.6462), maximum dV/dt (Pearson's r = -0.0637; p = 0.8081), or minimum dV/dt (Pearson's r = 0.1396; p = 0.5931).

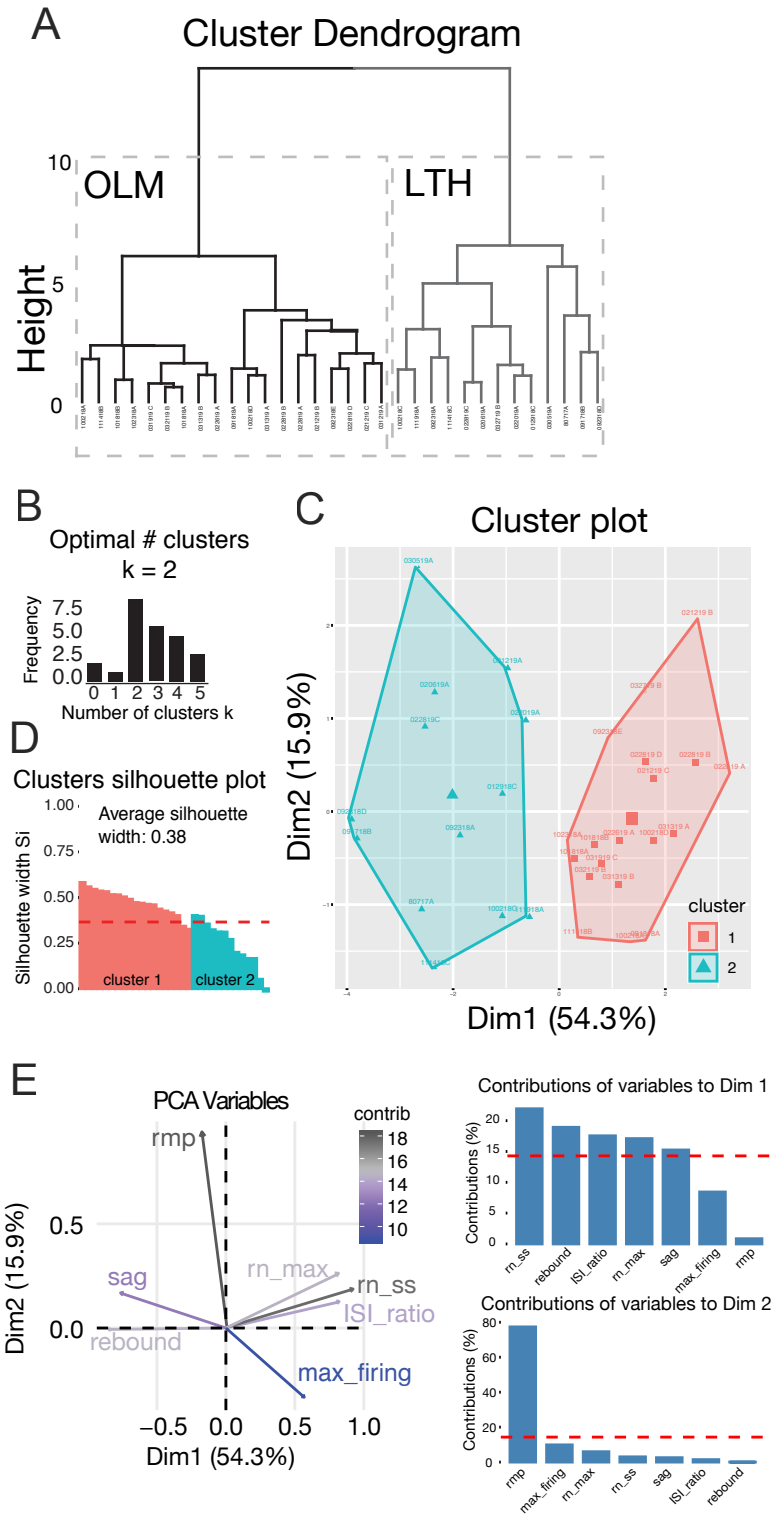

Figure 3: OLM and LTH cells separate into clusters based on intrinsic physiology
A. Cluster dendrogram of OLM and LTH cell clusters based on intrinsic electrophysiological properties. B. The optimal number of clusters indicated by NbClust in R Statistics, the optimal number of clusters for our data set k = 2. C. Cluster plot of principal component analysis (PCA) dimensions cluster 1 cells are LTH cells and cluster 2 cells are OLM cells. D. Silhouette plot of clusters 1 and 2. The average silhouette width was 0.38 E. Vector plot of PCA variables and their percent contribution to the clustering of OLM and LTH cells. Bar graphs show the contribution of variability to the two dimensions that carry a majority of the variability of the data set. Bars above the red line indicate variables that contribute more than the calculated average variability of any given parameter.

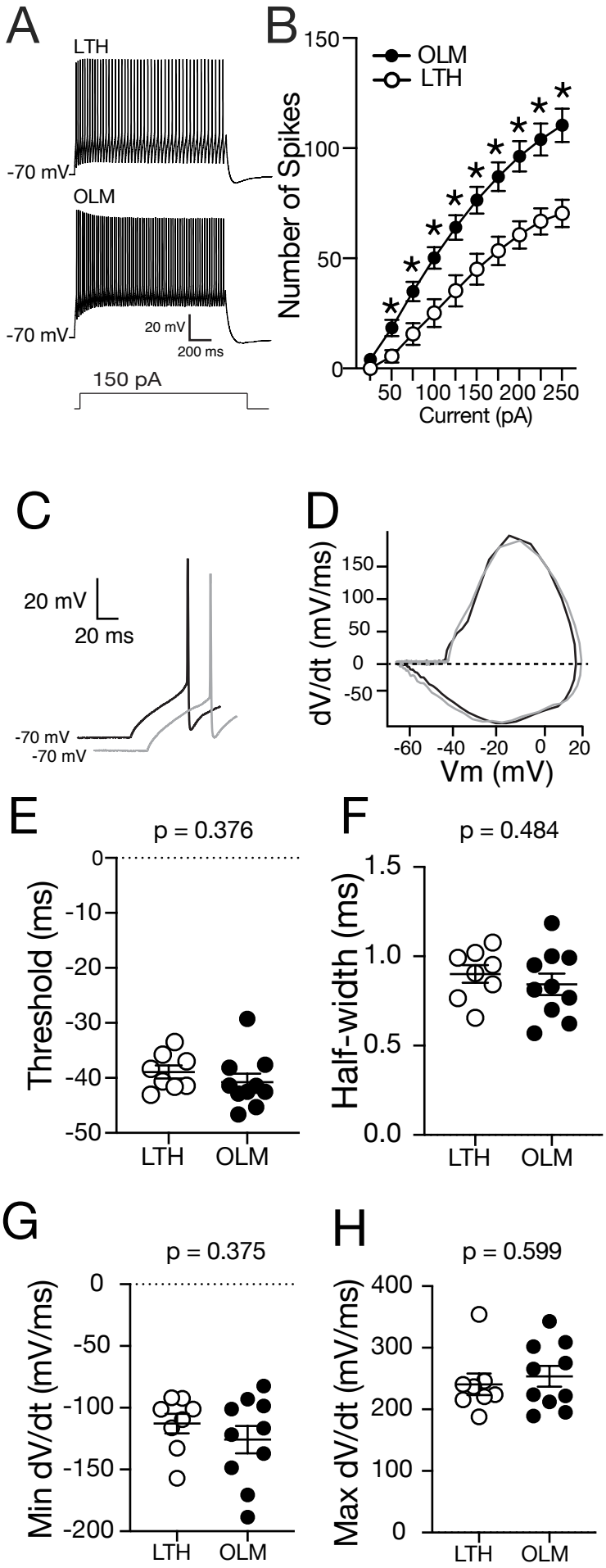

Figure 4: OLM have higher firing rates than LTH cells. A. Voltage traces showing action potential firing from an LTH and OLM cells in response to a 1.5 s, 150 pA current injection. B. Summary plot showing that OLM cells fire significantly more action potentials compared to LTH cells across a range of current injection amplitudes (repeated measures ANOVA, main effect of current ($F(9, 144) = 279.3$; $p = 0.0001$), main effect of cell type ($F(1, 16) = 13.12$; $p = 0.0023$), interaction between cell type and current ($F(9, 44) = 9.66$; $p = 0.0001$). C. First AP on which analysis was conducted. D. Phase plane plot of the first spike. E-H. Action potential threshold (E), half-width (F), minimum dV/dt (G) and maximum dV/dt (H) are not significantly different between LTH and OLM cells.

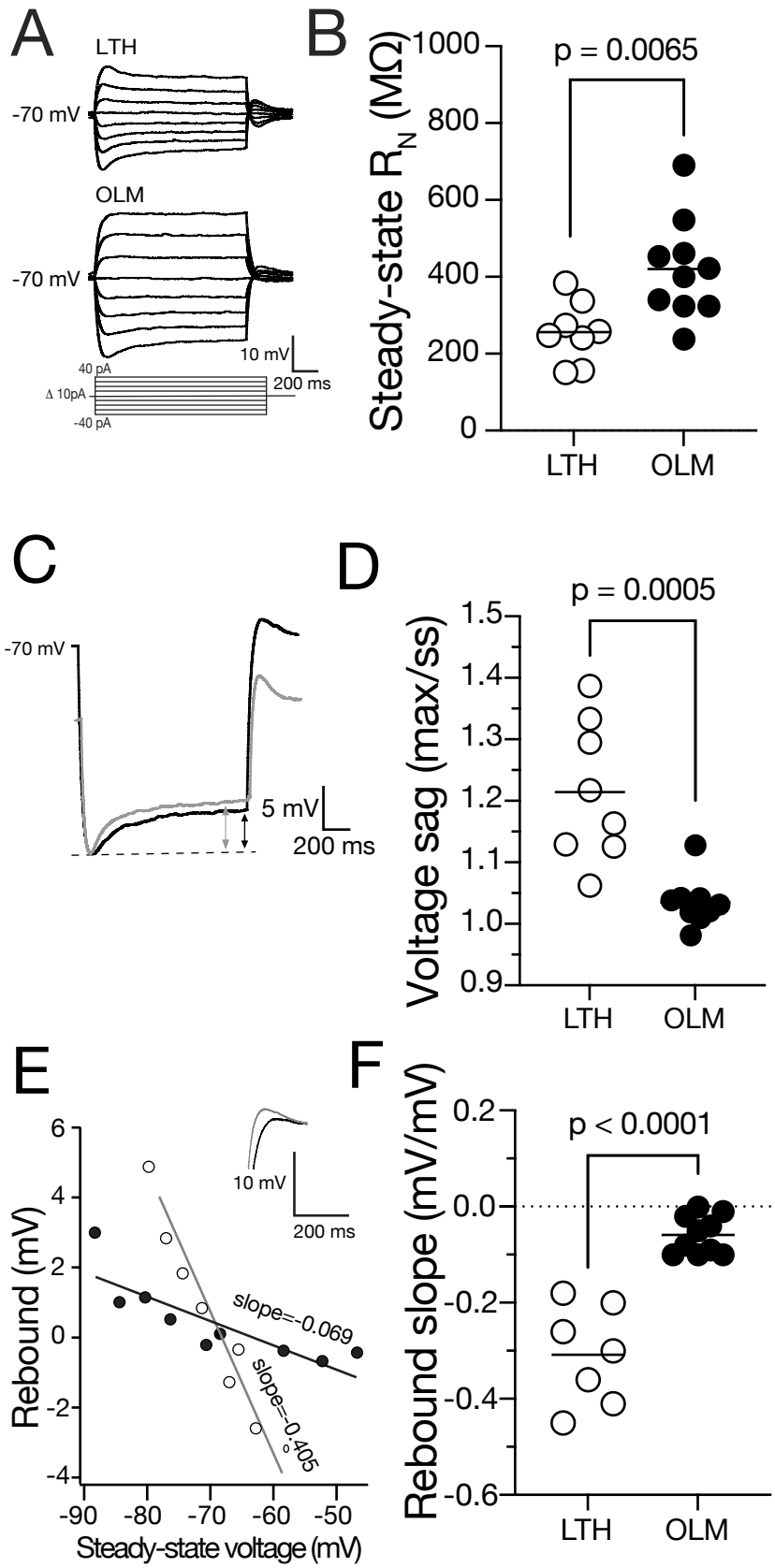

Figure 5: LTH cells have lower input resistance compared to OLM cells. A. Voltage responses to a family of subthreshold current injections from OLM and LTH cells. B. OLM cells have a significantly higher input resistance (RN) than LTH cells (unpaired t-test, p = 0.006). C. Voltage traces indicating the sag in LTH (grey) and OLM (black) cells. The arrows indicate the difference between the maximum voltage and the steady state of the cell. D. LTH cells have significantly higher sag compared to OLM cells (unpaired t-test, p < 0.001). E. Measurement of rebound in the traces seen in C and indicated by the traces of LTH (grey) and OLM (black) cell voltage traces of rebound. F. LTH cells have significantly more rebound than OLM cells (unpaired t-test, p < 0.001).

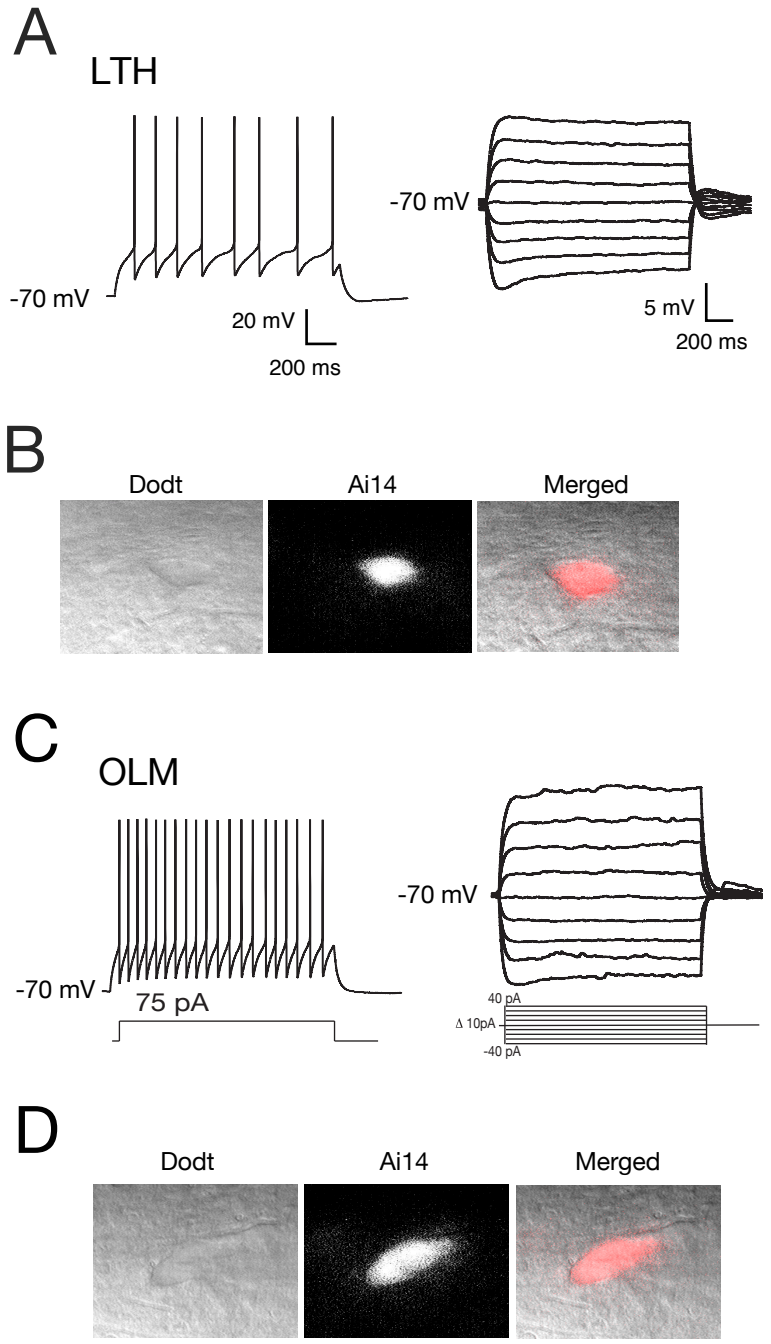

Figure 6: LTH and OLM cells are found in SST:cre Ai14 mice A. representative firing and subthreshold traces of an Ai14+ LTH neuron recording. (n = 7/13 recorded cells) B. LTH interneuron under Dodt contrast, expressing Ai14 driven florescence, and both images overlayed. C. representative firing and subthreshold traces for an Ai14+ OLM neuron recording. (n = 8/13 recorded cells) D. OLM neuron under Dodt contrast, expressing Ai14, and both images overlayed.

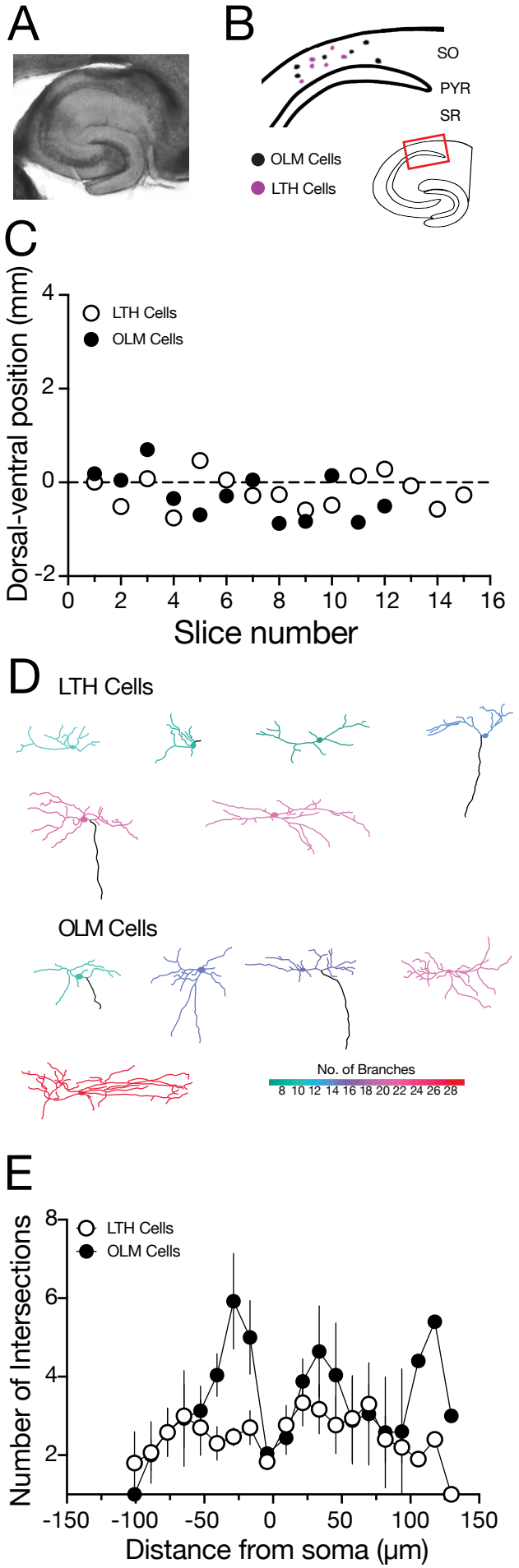

Figure 7: Dorsal/ventral position is not different between LTH and OLM cells, morphology. A. bright field image at 5x showing the CA1 area of the hippocampus. B. schematic of the location of fully recovered and reconstructed LTH and OLM cells recordings in the CA1 SO. Black indicates OLM cell body and pink indicates LTH cell body. C. Dorsal/ventral position of LTH and OLM cells from all slices used in experiments. D. Neuronal reconstructions of LTH and OLM cells. Black lines indicate the axon. The color coding indicates the number of branch points using the scale in the lower right corner. E. Scholl analysis of morphological constructions of LTH and OLM

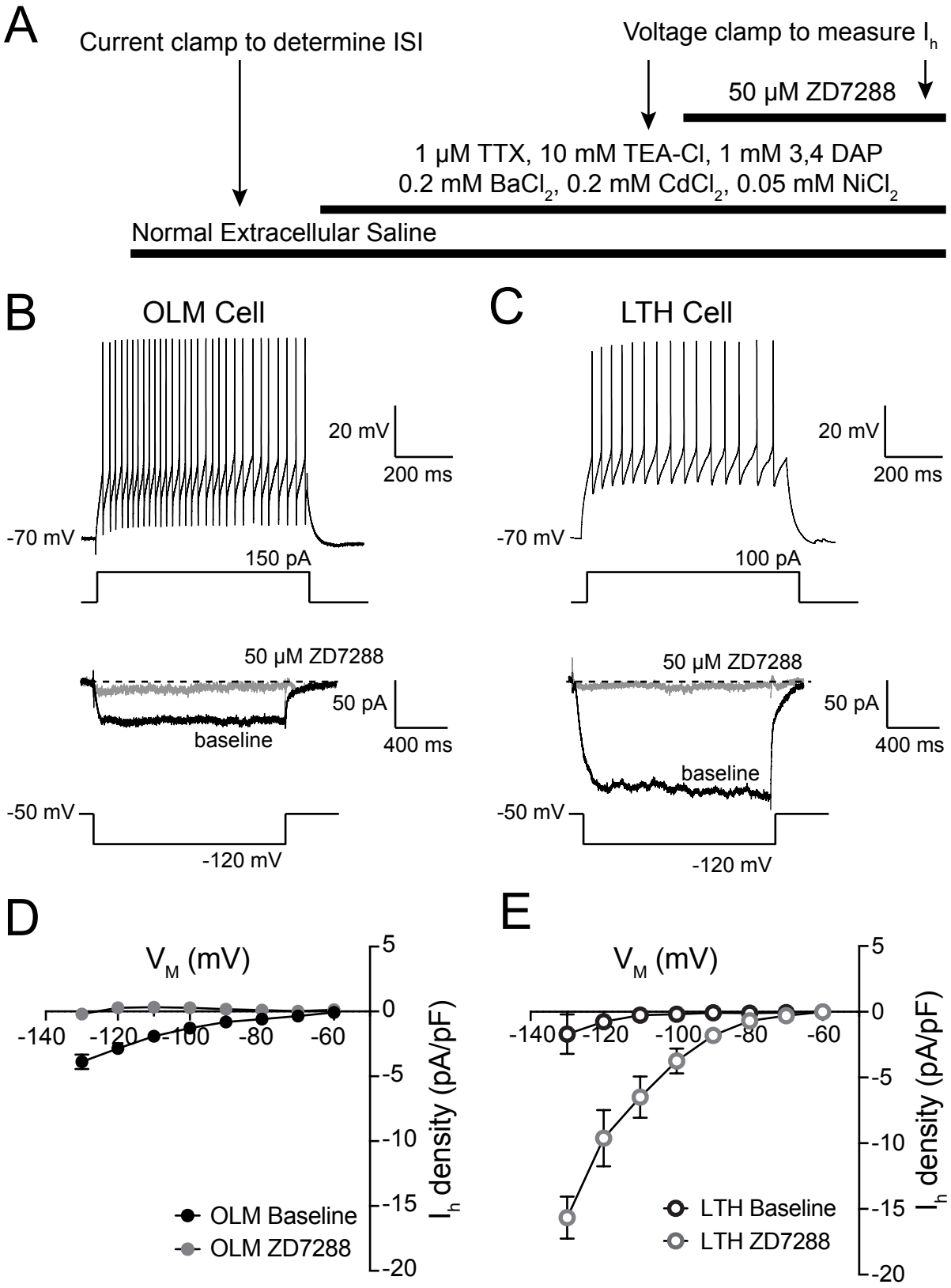

Figure 8: Ih density is higher in LTH cells. A. Experimental design for measuring Ih from OLM and LTH cells. B. Representative OLM cell showing action potential firing with high ISI ratio measured in current clamp (top) and Ih measured in voltage clamp (bottom). C. Representative LTH cell showing action potential firing with low ISI ratio measured in current clamp (top) and Ih measured in voltage clamp (bottom). D. Ih density before and after application of 50 μM ZD7288 in OLM cells. E. Ih density measured before and after application of 50 μM ZD7288in LTH cells.